Failure Criterion for Two-Ply Plain-Weave CFRP Laminates

H.M.Y.C. Mallikarachchi*, Sergio Pellegrino

Graduate Aerospace Laboratories, California Institute of Technology
1200 E. California Blvd MS 301-46, Pasadena, CA 91125

Abstract

We present an experimentally-based failure criterion for symmetric two-ply plain-weave laminates of carbon-fiber reinforced plastic. The criterion is formulated in terms of six force and moment stress resultants and consists of a set of three inequalities, related to in-plane, bending, and combined in-plane and bending types of failure. All failure parameters in the criterion are measured directly from five sets of tests. The new criterion is validated against an extensive data set of failure test results that use novel sample configurations to impose different combinations of stress resultants. It is found that the proposed criterion is safe for all test conditions and yet avoids excessive conservatism.

Keywords:
composite materials, failure criterion, plain weave, deployable structures

1. Introduction and Background

Predicting failure in composite materials is challenging. Even for the simple case of unidirectional laminates under in-plane loading conditions the recent World-Wide Failure Exercise [1] has shown that standard and now widely-used failure criteria have limited predictive accuracy. For woven laminates the situation is more complex as the weave geometry introduces stochastic variations in the distribution and arrangement of the fibers that are responsible for stress concentrations. These effects become more significant in thin laminates, i.e. laminates of only one or two plies, which are of particular interest for lightweight deployable space structures.

We have been working on stored-strain-energy composite deployable booms with tape-spring hinges made from a two-ply laminate of plain weave carbon fiber reinforced plastic (CFRP) and have developed high fidelity computer simulation techniques for folding and dynamic deployment of these booms. [2, 3] In these simulations the laminate is modeled as a Kirchhoff thin plate with elastic properties provided by its ABD stiffness matrix, which relates the mid-plane strains and curvatures to the corresponding force and moment resultants. This matrix, obtained from micro-mechanical homogenization, defines a continuum-shell model of the boom with which folding and deployment analyses were successfully carried out.

The results of this macro-level analysis can be used to determine in detail the stress and strain distribution in the representative volume element which, in combination with a failure criterion

*Currently at: Department of Civil Engineering, University of Moratuwa, Sri Lanka.
Email addresses: yasithcm@gmail.com (H.M.Y.C. Mallikarachchi), sergiop@caltech.edu (Sergio Pellegrino)

such as Tsai and Wu [4] or Hashin and Rotem [5], should be able to provide an estimate for the onset of failure at a point of the boom. This approach is well established and is generally known as Direct Micromechanics Method[6] but, when we applied it to the prediction of failure of two-ply laminates we obtained poor correlation between predictions and experiments.

The relevant literature on woven composites provides some useful clues but no definitive answer. Chou [7] summarizes various mechanics based models for stiffness and strength prediction of 2D and 3D woven composites. It reports that micro-mechanical models have been successfully employed in predicting thermoelastic properties but their use for strength prediction under multi-axial loading is still under development. Cox et al. [8] have developed a binary model which performs Monte Carlo simulations of failure under monotonic and fatigue loading. They have highlighted the importance of realistic representation of the pattern of reinforcing tows, random irregularity in tow positioning, randomness of the strengths of constituent elements and the mechanics of stress distribution around sites of local failure. Whitcomb and Srirengan [9] have shown that quadrature order and mesh refinement of the finite element model have a significant effect on the prediction of failure of plain weave composite subjected to in-plane extension. Song et al. [10] have shown that there is a significant difference between compressive failure strength obtained from a single unit cell and multiple unit cells, for two-dimensional braided textile composites.

Here we consider the laminate shown in Fig. 1 and present an alternative approach that formulates a stress-resultant failure criterion in terms of failure parameters directly measurable from five sets of tests. Our starting point is the quadratic polynomial criterion proposed by Karkkainen et al. [6], which was a generalization of the Tsai-Wu failure criterion to force and moment resultant space. Karkkainen et al. [6] estimated the parameters that define this failure criterion with finite element calculations carried out on a representative unit cell, and used the Tsai-Wu criterion to define point-wise failure conditions. An analogous approach, but using a strain based criterion was adopted by Manne and Tsai [11] in the design optimization of composite plates.

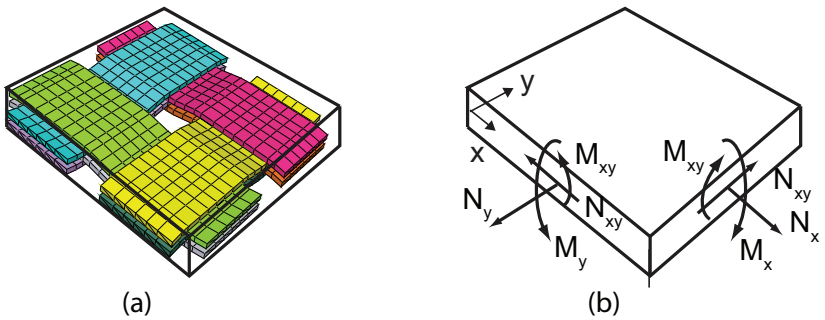

Figure 1: (a) Repeating unit cell of two-ply plain weave laminate and (b) definition of stress resultants for homogenized plate model.

The failure criterion proposed by Karkkainen et al. [6] can be expressed in the general form

$$f_i\sigma_i + f_{ij}\sigma_i\sigma_j = 1 \tag{1}$$

where $\sigma_i = N_x, N_y, N_{xy}, M_x, M_y, M_{xy}$ for $i = 1, \ldots, 6$ are the stress resultants defined in Fig. 1. The parameters f_i and f_{ij} represent respectively 6 and 21 (note that $f_{ij} = f_{ji}$) failure coefficients such that Equation 1 defines a failure condition when its magnitude exceeds 1. The parameters f_i and the diagonal terms f_{ii} correspond to individual loading conditions in which only one stress resultant is non-zero; the non-diagonal terms f_{ij} with $i \neq j$, deal with coupling between different stress resultants.

Due to the four-fold rotational symmetry about the z-axis of the laminate, the parameters f_i and f_{ij} should not change if x and y are exchanged. This is equivalent to requiring $f_1 = f_2$, $f_4 = f_5$ and $f_{11} = f_{22}$, $f_{44} = f_{55}$, $f_{13} = f_{23}$, $f_{14} = f_{15} = f_{24} = f_{25}$, $f_{16} = f_{26}$, $f_{34} = f_{35}$, $f_{46} = f_{56}$. These equalities reduce the 27 failure coefficients to only 16.

The same four-fold symmetry also requires the strength of the laminate to be *independent of the sign of the in-plane shearing and twisting resultants* and it can also be shown that the strength of the laminate is independent of the sign of the out-of-plane bending moment. Because the laminate is not symmetric with respect to its xy mid-plane, this last property can be shown by considering an alternative unit cell that is translated by half the width of the unit cell shown in fig. 1a, and then arguing that since both unit cells have the same bending strength its magnitude has to be independent of the sign of the moment. Thus it is concluded that all parameters that multiply a linear term in N_{xy}, M_x, M_y, or M_{xy} should also vanish and this condition sets $f_i = 0$ for $i = 3, \ldots 6$ and $f_{ij} = 0$ for $i = 1, \ldots, 6$ and $j > i$, apart from f_{12}.

The net outcome of the stated symmetry conditions is that there are only 6 non-zero failure parameters: $f_1 = f_2$, $f_{11} = f_{22}$, f_{12}, f_{33}, $f_{44} = f_{55}$, f_{66} and so the failure criterion has the expression:

$$f_1(N_x + N_y) + f_{11}(N_x^2 + N_y^2) + f_{12}N_xN_y + f_{33}N_{xy}^2 + f_{44}(M_x^2 + M_y^2) + f_{66}M_{xy}^2 = 1 \tag{2}$$

where the failure parameters can be obtained as follows. It should be noted that Karkkainen et al. [6] considered only the symmetry conditions $f_i = 0$ for $i = 3, \ldots 6$ in defining their locus.

Consider a purely tensile loading condition for the laminate, where the load is acting in the x-direction and F_{1t} is the measured tensile strength. Substituting $N_x = F_{1t}$ and $N_y = N_{xy} = M_x = M_y = M_{xy} = 0$ into Equation 2 gives

$$f_1F_{1t} + f_{11}F_{1t}^2 = 1 \tag{3}$$

Similarly, consider a purely compressive loading in the x-direction and denote by F_{1c} the measured compressive strength. Substituting $N_x = -F_{1c}$ and $N_y = N_{xy} = M_x = M_y = M_{xy} = 0$ into Equation 2 gives

$$-f_1F_{1c} + f_{11}F_{1c}^2 = 1 \tag{4}$$

Equations 3 and 4 can be solved for f_1 and f_{11}

$$f_1 = \frac{1}{F_{1t}} - \frac{1}{F_{1c}} \tag{5a}$$

$$f_{11} = \frac{1}{F_{1t}F_{1c}} \tag{5b}$$

Similarly, considering pure shear, bending and twisting loading conditions one finds that

$$f_{33} = \frac{1}{F_3^2} \tag{6a}$$

$$f_{44} = \frac{1}{F_4^2} \tag{6b}$$

$$f_{66} = \frac{1}{F_6^2} \tag{6c}$$

where F_3, F_4 and F_6 are respectively the measured strengths in shear, bending and twisting.

The last failure coefficient, f_{12}, is in general difficult to determine experimentally. Liu and Tsai [12] have shown that for typical carbon and glass fiber composites it can vary between -0.9 $\sqrt{f_{11}f_{22}}$ and 0. They have also shown that a reasonable approximation is

$$f_{12} = -\frac{\sqrt{f_{11}f_{22}}}{2} \tag{7}$$

which is referred to as generalized von Mises model.

In conclusion, incorporating the previously noted symmetry conditions, the failure coefficients are given by:

$$f_1 = f_2 = \frac{1}{F_{1t}} - \frac{1}{F_{1c}} \tag{8a}$$

$$f_{11} = f_{22} = \frac{1}{F_{1t}F_{1c}} \tag{8b}$$

$$f_{12} = -\frac{f_{11}}{2} \tag{8c}$$

$$f_{33} = \frac{1}{F_3^2} \tag{8d}$$

$$f_{44} = f_{55} = \frac{1}{F_4^2} \tag{8e}$$

$$f_{66} = \frac{1}{F_6^2} \tag{8f}$$

where F_i represent directly measured strengths in the tow directions of the laminate, and the subscripts t and c denote tension and compression, respectively.

In the next section we will present a set of five test configurations that provide the required failure strengths, plus an additional set of five tests to measure the failure strengths under the action of combined stress resultants. These additional results provide experimental data that will be used to validate the failure criterion. The results from these tests are presented in Section 3. Then, in Section 4 it is shown that the quadratic criterion in Equation 2 is unable to fully capture the interaction between stress resultants and thus a new failure criterion is proposed in Section 5. The parameters for the new criterion are still obtained from the original set of five failure strengths but the new criterion works much better for all combined loading cases. Section 6 discusses the new failure criterion and Section 7 concludes the paper.

2. Strength Measurements

Useful background to the tests presented in this section is provided in Masters and Portanova [13]. Also, ASTM D6856 [14] provides general guidelines for testing textile composites as well as some changes that should be made before using standards developed for unidirectional laminates.

The strength properties of two-ply T300-1k/Hexcel 913 plain weave laminates were characterized by means of a range of failure tests on sets of nominally identical samples. All laminates were made by impregnating T300-1k [15] plain weave dry fabric with Hexcel 913 [16] epoxy resin. Lay-ups of resin impregnated fabric were cut to the required dimensions and cured in an autoclave under vacuum for 1 h at 125°C and under a pressure of 600 kPa. The fiber volume fraction of the samples was 0.62, the areal density 280 g/mm^2 and the average thickness 0.22 mm.

All tests were done on an Instron 5569 materials testing machine, using either a 50 kN or a 1 kN load cell. All strain measurements were made with Epsilon LE01 and LE05 laser extensometers.

Figure 2 shows the material directions, x and y, aligned with the tows and the loading directions x' and y', at an angle ϕ to x and y. Note that if x' and y' coincide with x and y, they will be denoted as x and y. Next we describe the test configurations and measurement system to obtain failure data in the x', y' coordinate system. These results will then be converted to material coordinates in Section 3.

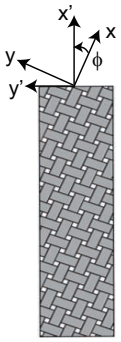

Figure 2: Definition of material and loading directions.

2.1. Tension Tests

The tension tests were conducted according to ASTM D3039 [17]. Six 227 mm long and 25 mm wide specimens were reinforced with 50 mm long by 25 mm wide aluminum-alloy end tabs with 5° bevel angle, bonded to the sample with high strength adhesive Devcon Plastic Welder. Two pairs of retro-reflective strips were attached near the center of the exposed region, at gauge lengths of 50 mm and 15 mm respectively to measure the longitudinal and transverse strains.

Each sample was connected to the testing machine with wedge clamping jaws and was pulled at a rate of 2 mm/min while measuring the load with a 50 kN load cell. A few additional samples

were subjected to four cycles with maximum load of 80% of failure to confirm linearity and lack of hysteresis.

2.2. Compression Tests

Standard compression test procedures are not applicable to thin composites as failure would occur by macroscopic buckling. Hence, following Fleck and Sridhar [18], the compression tests were performed on short sandwich columns where two-ply laminate face skins are bonded to a foam core. The geometry of the columns and the stiffness of the foam core are chosen such as to achieve failure by fiber microbuckling while avoiding both global and local (face-sheet) buckling [18]. The test samples were made by bonding two 60 mm long by 40 mm wide composite face sheets to 12.5 mm thick Divinicell H200 PVC foam core with Devcon Plastic Welder. U-shaped aluminum-alloy end caps were held parallel and perpendicular to the sample and were bonded to it, Figure 3a, to achieve a uniform load distribution across the two faces.

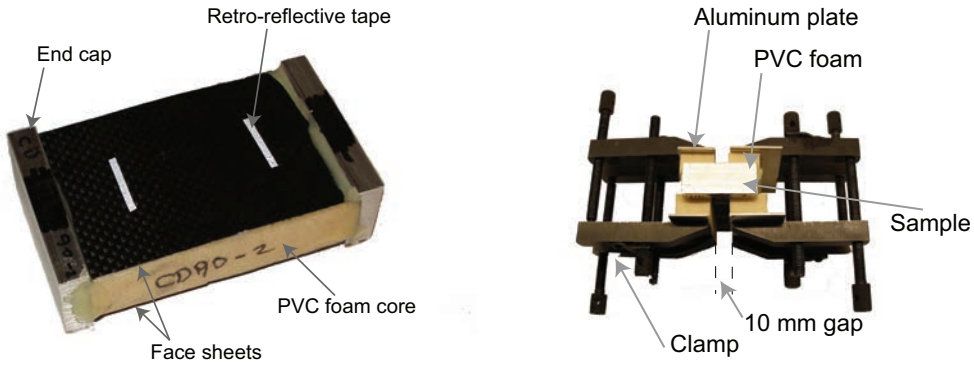

(a) Compression sample

(b) Lateral support system

Figure 3: Compression test.

During the test, lateral supports were provided to prevent the face sheets from debonding from the core, by pressing four PVC foam blocks with 1 mm thick aluminum-alloy plates against the face sheets, as shown in Figure 3b. These blocks left 10 mm wide central gaps, through which the extensometers measured the extension of the face sheets. The samples were loaded at a rate of 0.06 mm/min while measuring the applied load with the 50 kN load cell.

2.3. Shear Tests

These tests were carried out according to the ASTM D3518 $[\pm 45]_{ns}$ shear test method [19] which has been developed for measuring the shear strength of a lamina. Since this test applies biaxial tension in addition to shear, a correction has to be made for estimating the strength in pure shear. The details will be explained in Section 3.3.

Ten two-ply ±45 samples with the same dimensions of the tension samples described in Section 2.1 were made. However, the ends were covered with 50 mm long emery cloth tabs instead of aluminum-alloy tabs. Two retro-reflective strips were attached 50 mm and 15 mm apart, respectively for the longitudinal and transverse strain measurements. Each sample was pulled under tension at a rate of 2 mm/min until failure.

2.4. Bending Tests

Standard three-point or four-point flexural strength tests are not applicable for thin laminates, because their elastic deformation range is too large. Instead, the platen folding test [20],[21] was used to determine the smallest radius to which the laminate can be folded before failure and the corresponding bending moment. 100 mm long by 50 mm wide specimens were attached to two flat aluminum-alloy plates connected to the testing machine, Figure 4. The top platen was moved down at a rate of 2 mm/min, while recording the applied force with a 1 kN load cell. Images of the test sample were taken with a Sony Handycam HDR-XR500V digital video camera, at a rate of 30 frames per second. The last image taken prior to failure was used to measure the failure radius r_x and the corresponding moment M_x was obtained from the known geometry at failure and the measured applied force at failure.

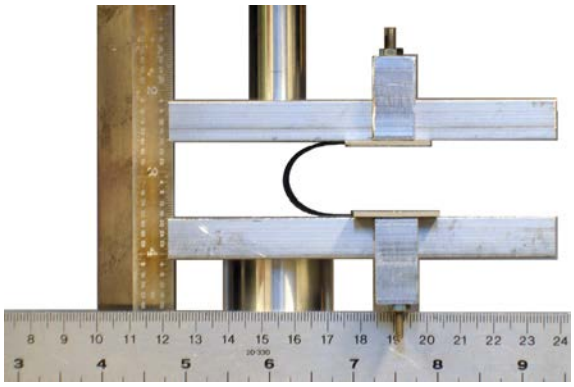

Figure 4: Platen folding test setup.

2.5. Twisting Tests

It is impractical to measure the twisting moment at failure of a thin laminate by applying large torsional rotations, as twisting would induce rapidly increasing non-linear mid-plane stretching. Instead, an off-axis bending test configuration was selected, based on the platen folding test described in Section 2.4. This test was carried out on five two-ply ±45 laminates and five two-ply 30/-60 laminates. Due to the off-axis fiber orientation of the samples, a twisting moment is applied in the tow directions, together with biaxial bending moments. An analysis of these moments is presented in Section 3.5.

2.6. Combined Loading Tests

The test configurations described in Sections 2.1-2.5 can be applied to initially curved and/or off-axis samples to set up combined loading conditions. For example, by flattening an initially curved sample and then taking it to failure under tension or bending allows us to determine the axial force or bending moment at failure in the presence of a constant moment preload. The level of preload can be varied by testing specimens with different initial radii. Additional tests were carried out on samples with off-axis fiber directions, to introduce a combination of either axial and shear loading or bending and twisting.

2.6.1. In-Plane Loading

Off-axis tension tests are commonly used as biaxial loading tests to verify material properties determined with standard uniaxial tests [22]. Five $[30/\text{-}60]_2$ samples were tested; the sample configuration and test procedure were similar to the shear tests described in Section 2.3, but this time a combination of biaxial and shear loads was applied.

2.6.2. Coupled In-Plane and Bending Loading

This type of coupling was achieved by performing tension tests on two-ply 0/90 specimens that were initially curved either in the longitudinal or transverse direction, Figure 5a.

All samples were 125 mm long and 25 mm wide, with 25 mm long emery cloth tabs glued to each end. This provides a 75 mm clear region to measure the longitudinal and transverse strains across two pairs of retro-reflective strips, at distances of 25 mm and 15 mm. The length of the samples was limited by the maximum length of prepreg that could be wound on a cylindrical mandrel. However, note that the clear test length included on the order of of 29 repeating unit cells, where the length of a unit cell is 2.66 mm. ASTM D6856 [14] recommends that the gauge area should be larger than at least two unit cells. Also note that the retro-reflective strips were placed sufficiently far away from the supports to minimize edge effects.

First, each sample was loaded under four-point bending to measure the moment required to remove the initial curvature, Figure 5b. After this initial bending test, the sample was set up for a tension test and pulled at a rate of 2 mm/min until failure. This test was carried out on three sets of respectively 5, 7, and 3 curved specimens with radii r_x = 19.1, 25.4 and 38.1 mm, to measure the interaction between N_x and M_x. A further sets of tests was carried out on samples with initial transverse radii r_y = 25.4 and 38.1 mm, to measure the interaction between N_x and M_y. The transverse moment was assumed to be equal to the longitudinal moments with the same longitudinal radii that had been previously measured.

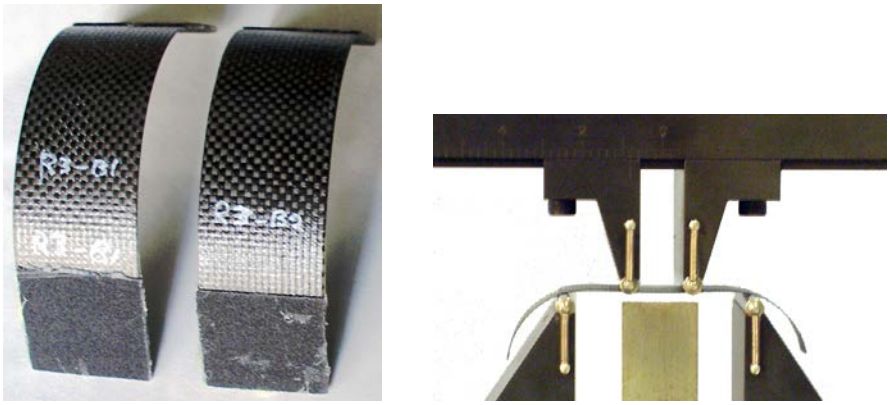

(a) Longitudinally curved sample (b) Straightened-up sample

Figure 5: Coupled axial-bending tests.

2.6.3. Coupled Shear and Twist Loading

Longitudinally curved two-ply ±45 samples with $r_{x'}$ = 38.1 mm were tested in shear as described in Section 2.3. This configuration applies all six stress resultants simultaneously, and different twisting moment preloads are applied by varying the initial curvature of the sample.

2.6.4. Coupled Biaxial Bending

The bending test configuration described in Section 2.4 can be applied to 0/90 and ±45 transversely curved samples to impose biaxial bending conditions. These samples were first flattened and then subjected to longitudinal bending in the platen folding test, up to failure. The initial curvature and the curvature applied during the test were in the opposite sense and hence the curvature changes were of the same sign. These tests were carried out by Yee and Pellegrino [23] and Yee [24], on the same laminates that are investigated in the present study, but cured with LTM45 epoxy resin instead of Hexcel 913. Since there are no significant differences in the properties of these two resins the tests were not repeated, instead it was decided to use the published results.

2.6.5. Coupled Bending and Twist Loading

The biaxial bending test described in Section 2.6.4 on an off-axis sample applies both biaxial bending and twisting in the material directions. Hence, this test configuration was applied to two-ply ±45 samples with transverse radii $r_{y'} = 25.4$ and 38.1 mm.

3. Experimental Results

This section analyzes the results obtained from the experiments described in Section 2. For each experiment the sample average, $\bar{x}$, standard deviation, s_{n-1}, and coefficient of variation, CV, were determined. These parameters are defined as

$$\bar{x} = \frac{\sum_{i=1}^{n} x_i}{n} \tag{9a}$$

$$s_{n-1} = \sqrt{\frac{\sum_{i=1}^{n} x_i^2 - n\bar{x}^2}{(n-1)}} \tag{9b}$$

$$CV = \frac{100 \times s_{n-1}}{\bar{x}} \ \% \tag{9c}$$

where x_i is a general measured or derived property and n is the number of tested samples. Note that, because of the brittle failure type that we are dealing with, for each set of tests the corresponding failure strength will be simply taken as the *minimum value* obtained from that set.

Since we are dealing with sets the full set of plate stress resultants and only a limited number of them can be determined from direct measurements, the standard elastic relationship between out-of-plane stress resultants and the corresponding deformation variables will be used to determine any stress resultants that cannot be measured. Modeling the laminate as a thin Kirchhoff plate and introducing a single correcting factor to account for geometry change effects in the laminate near failure, this relationship has the form

$$\begin{Bmatrix} \Delta M_{x'} \\ \Delta M_{y'} \\ \Delta M_{x'y'} \end{Bmatrix} = \alpha \begin{bmatrix} D_{11} & D_{12} & D_{16} \\ D_{21} & D_{22} & D_{26} \\ D_{61} & D_{62} & D_{66} \end{bmatrix} \begin{Bmatrix} \Delta \kappa_{x'} \\ \Delta \kappa_{y'} \\ \Delta \kappa_{x'y'} \end{Bmatrix} \tag{10}$$

where the three by three constitutive matrix is the D matrix for the plate and α is a stiffness reduction factor that is obtained experimentally. Its values are 0.6, 0.67 and 0.8, respectively for 0/90, 30/-60 and ±45 laminates, see Sections 3.4 and 3.5 for details.

Experimentally validated D matrices for two-ply T300-1k/Hexcel 913 plain weave 0/90 laminate were obtained in Mallikarachchi and Pellegrino [2]. Assuming the tows in the two plies to be in-phase[25] the following matrix was obtained:

$$D^0 = \begin{pmatrix} 41.3 & 1.5 & 0 \\ 1.5 & 41.3 & 0 \\ 0 & 0 & 2.3 \end{pmatrix} \tag{11}$$

Standard transformations provide the ABD matrices for the two-ply ±45 and 30/60 laminates:

$$D^{45} = \begin{pmatrix} 23.6 & 19.1 & 0 \\ 19.1 & 23.6 & 0 \\ 0 & 0 & 19.9 \end{pmatrix} \tag{12}$$

and

$$D^{30} = \begin{pmatrix} 28.0 & 14.7 & 0 \\ 14.7 & 28.0 & 0 \\ 0 & 0 & 15.5 \end{pmatrix} \tag{13}$$

The units are N and mm for all of these matrices.

3.1. Tensile Strength

Figure 6 shows the typical N_x vs. ε_x response obtained from the tension tests and Table 1 summarizes the failure values that were obtained. Note that failure occurred at multiple locations (failure code LMV in ASTM D3039 [17]). The cases in which failure occurred near the ends of a sample are likely to have provided a lower bound on the actual strength, the smallest measurement was taken to define the strength of the laminate.

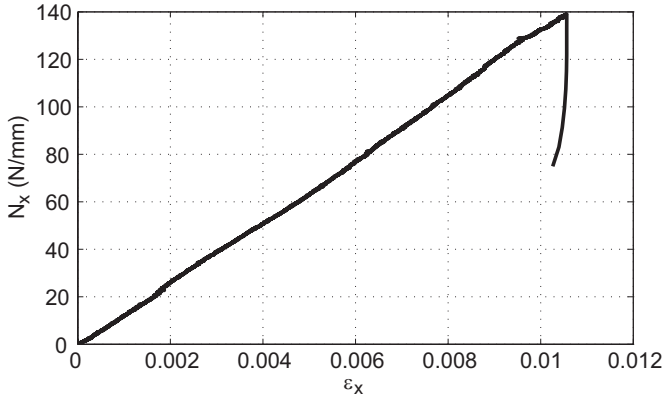

Figure 6: Typical tensile response.

The tensile strength is the smallest failure value reported in Table 1, hence:

$$F_{1t} = F_{2t} = 133.60 \text{ N/mm} \tag{14}$$

Sample	ε_x (%)	N_x (N/mm)
TD90-1	0.96	133.60
TD90-2	1.05	135.80
TD90-3	1.06	143.20
TD90-4	1.04	141.00
TD90-5	1.01	138.50
TD90-6	0.99	144.70
$\bar{x}$	1.02	139.47
s_{n-1}	0.04	4.30
CV (%)	3.80	3.08

Table 1: Tensile failure data.

3.2. Compressive Strength

The compressive failure strength is measured when failure occurs by fiber microbuckling, Figure 7, however it should be noted that in a sandwich column it is quite rare for microbuckling of both face sheets to occur simultaneously. Hence only the extensometer reading for the failed side was considered and the failure stress-resultant was calculated by assuming that both sheets had been equally loaded. This value was modified to account for the load taken by the foam core, which is

$$N_x = \frac{P - \sigma_{core} A_{core}}{2w} \tag{15}$$

where, σ_{core} is the stress in the core that corresponds to the measured failure strain of the sandwich column, obtained from the stress-strain response curve for Divinicell H200 PVC foam, in [18] where P, A, and w denote the total applied force, cross-sectional area, and width of the column, respectively.

Figure 7: Fiber microbuckling.

Figure 8 shows the response of both faces of a single sandwich column. The particular test shown gave the closest agreement among the two faces of any samples, however the failure

strengths obtained for other samples were also comparable, Table 2.

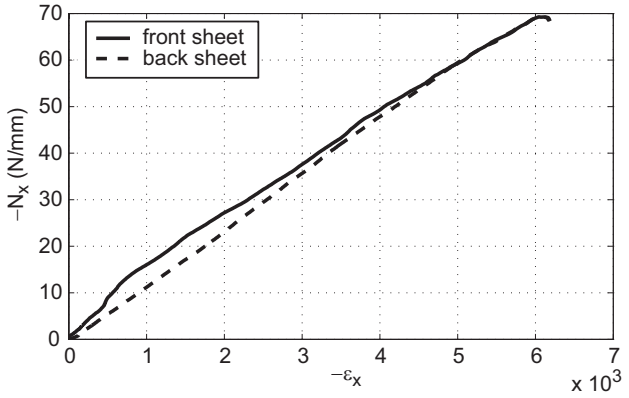

Figure 8: Compressive response measured on both sides of a specimen.

Sample	$\lvert\varepsilon_x\rvert$ (%)	$\lvert N_x\rvert$ (N/mm)
CD90-1	0.69	63.23
CD90-2	0.70	77.89
CD90-3	0.61	67.50
CD90-4	0.64	60.56
CD90-5	0.59	57.36
CD90-6	0.66	64.96
CD90-7	0.49	59.50
CD90-8	0.56	59.49
CD90-9	0.56	60.39
CD90-10	0.61	63.66
$\bar{x}$	0.61	63.42
s_{n-1}	0.06	5.75
CV (%)	10.59	6.10

Table 2: Compressive failure data

The compressive strength is the smallest failure value reported in Table 2, hence:

$$F_{1c} = F_{2c} = 57.36 \text{ N/mm} \tag{16}$$

3.3. Shear Strength

Table 3 lists the measured tensile strengths of all two-ply ±45 specimens that were tested. The force resultants in the tow directions can be obtained from $N_{x'}$ with the transformation

$$N_x = \cos^2\phi\, N_{x'} \tag{17a}$$

$$N_y = \sin^2\phi\, N_{x'} \tag{17b}$$

$$N_{xy} = \sin\phi\cos\phi\, N_{x'} \tag{17c}$$

from which

$$N_{xy} = \frac{N_{x'}}{2} \tag{18}$$

The shear strain is also calculated by a coordinate transformation, as follows:

$$\gamma_{xy} = \varepsilon_{x'} - \varepsilon_{y'} \tag{19}$$

A typical shear response, obtained by applying the transformation in Equation 19 to the measurements obtained from an actual test, is shown in Figure 9.

Sample	$N_{x'}$ (N/mm)	$N_x = N_y = N_{xy}$ † (N/mm)
TD45-1	39.56	19.78
TD45-2	39.54	19.77
TD45-3	41.70	20.85
TD45-4	38.54	19.27
TD45-5	42.40	21.20
TD45-6	40.26	20.13
TD45-7	39.00	19.50
TD45-8	38.34	19.17
TD45-9	38.84	19.42
TD45-10	38.58	19.29
$\bar{x}$	39.68	
s_{n-1}	1.39	
CV (%)	3.50	

Table 3: Tensile strength of two-ply ±45 laminate († Values obtained from calculation).

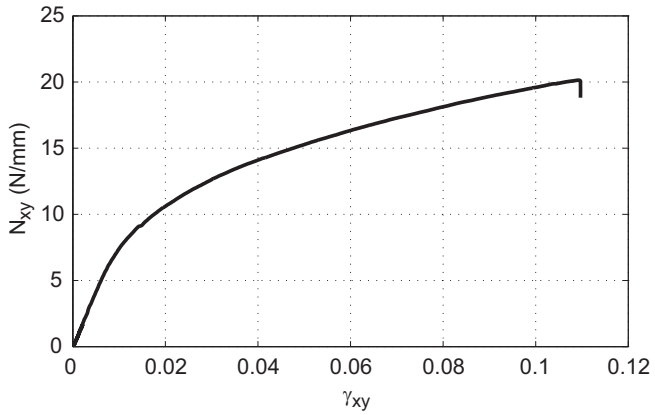

Figure 9: Typical shear response.

To determine the shear strength of the laminate it should be noted that in the chosen test configuration the samples were subjected to the stress resultants N_x and N_y, in addition to N_{xy}. This

biaxial loading is usually neglected for ±45 specimens made of unidirectional laminas [22], but in the present case we can use the failure criterion to estimate the pure shear strength by removing the effects of the normal stress resultants. From Equation 17 the in-plane stress resultants in the tow directions are $N_x = N_y = N_{xy} = N_{x'}/2$ and the moments are all zero. Hence, substituting these values into Equation 2, solving for f_{33} and then using Eq. 8 to evaluate F_3 we obtain

$$F_3 = \frac{1}{\sqrt{f_{33}}} = \frac{|N_{x'}|}{\sqrt{4 - (4f_1 N_{x'} + (2f_{11} + f_{12})N_{x'}^2)}} \tag{20}$$

Hence the shear strength is calculated from Eq. 20 with the smallest value of $N_{x'}$ in Table 3, which gives:

$$F_3 = 16.91 \text{ N/mm} \tag{21}$$

3.4. Bending Strength

In the platen test configuration the maximum moment and curvature occur at the mid point of the sample, as shown schematically in Figure 10. Sanford et al. [26] have shown that the curve formed by an initially flat thin sample folded between two parallel platens is accurately described by the elastica. Hence, the curvature at failure can be calculated by measuring the distance between the two platens, δ, from the image taken just before failure and the failure moment can be calculated from [26]

$$\kappa_{x'} = \frac{2.3963}{\delta} \tag{22}$$

$$M_{x'} = \frac{0.8346\, P\delta}{w} \tag{23}$$

where P denotes the force just prior to failure and w is the width of the sample.

The transverse moment, $M_{y'}$ can be estimated by substituting $\Delta\kappa_{x'} = \kappa_{x'}$, $\Delta\kappa_{y'} = \Delta\kappa_{x'y'} = 0$ (where $\kappa_{x'}$ is obtained from Equation 22) into Equation 10. It turns out that even assuming $\alpha = 1$ for simplicity, in the case of two-ply 0/90 test samples the transverse moments are on the order of 4% of the longitudinal moments and hence can be neglected.

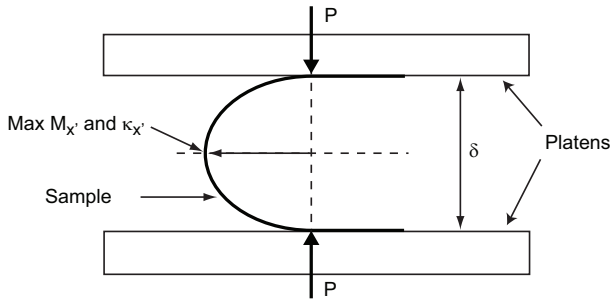

Figure 10: Schematic diagram showing platen test sample configuration near failure.

Table 4 presents the failure moments and curvatures obtained from platen folding tests performed on two-ply 0/90 test samples. From these data, the bending strength is given by the

smallest failure value listed, hence:

$$F_4 = F_5 = 4.54 \text{ Nmm/mm} \tag{24}$$

Sample	κ_x (1/mm)	M_x (Nmm/mm)
BDF90-1	0.218	5.021
BDF90-2	0.210	4.538
BDF90-3	0.200	5.118
BDF90-4	0.203	5.528
BDF90-5	0.187	4.990
BDF90-6	0.204	5.098
BDF90-7	0.202	5.180
$\bar{x}$	0.203	5.068
s_{n-1}	0.010	0.293
CV (%)	4.72	5.79

Table 4: Bending failure data for two-ply 0/90 samples.

Comparing the values of M_x in Table 4 with the values obtained by substituting the corresponding values of κ_x, also in Table 4, into Eq. 10 with the D matrix in Eq. 11 we determine the average stiffness reduction factor for 0/90 samples, $\alpha_0 = 0.6$.

3.5. Twisting Strength

The platen folding tests described in Section 2.5 were carried out on initially flat two-ply ±45 and 30/-60 laminates and the failure curvature $\kappa_{x'}$ and bending moments $M_{x'}$ were obtained after each test, as explained in Section 3.4. The results are presented in columns 2 and 3 of Tables 5 and 6.

In the present case $M_{y'}$ is not negligible. Its value is obtained by substituting $\Delta\kappa_{x'} = \kappa_{x'}$, $\Delta\kappa_{y'} = \Delta\kappa_{x'y'} = 0$ into Equation 10, where α was estimated by comparing $M_{x'}$ from Equation 10 with the measured $M_{x'}$ from Table 5. Thus it was found that on average $\alpha_{\pm 45} = 0.80$ and $\alpha_{30} = 0.67$. The results of these calculations have been presented in column 4 of Tables 5 and 6.

Once $M_{x'}$ and $M_{y'}$ are known they can be transformed to the tow directions with the transformations

$$M_x = \cos^2\phi\, M_{x'} + \sin^2\phi\, M_{y'} \tag{25a}$$

$$M_y = \sin^2\phi\, M_{x'} + \cos^2\phi\, M_{y'} \tag{25b}$$

$$M_{xy} = \sin\phi\cos\phi\, (M_{y'} - M_{x'}) \tag{25c}$$

and the results are presented in columns 5 and 6 of Table 5 and in columns 5, 6 and 7 of Table6.

These equations confirm that the samples were subjected to bending resultants in addition to M_{xy}, and hence this is not a pure twisting experiment. The procedure to obtain the pure twisting strength is to substitute the values of all six stress resultants at failure into Equation 2. Since the in-plane stress resultants are zero we have

Sample	$\kappa_{x'}$ (1/mm)	$M_{x'}$ (Nmm/mm)	$M_{y'}$† (Nmm/mm)	$M_x = M_y$† (Nmm/mm)	M_{xy}† (Nmm/mm)
BD45-1	0.281	5.113	3.488	4.300	-0.813
BD45-2	0.262	5.357	3.654	4.506	-0.851
BD45-3	0.278	5.265	3.591	4.428	-0.837
BD45-4	0.280	4.942	3.371	4.157	-0.785
BD45-5	0.283	5.794	3.952	4.873	-0.921
$\bar{x}$	0.277	5.294	3.611		
s_{n-1}	0.008	0.321	0.270		
CV (%)	3.01	6.06	6.06		

Table 5: Bending failure data for two-ply ±45 laminates († Values obtained from calculation).

Sample	$\kappa_{x'}$ (1/mm)	$M_{x'}$ (Nmm/mm)	$M_{y'}$† (Nmm/mm)	M_x† (Nmm/mm)	M_y† (Nmm/mm)	M_{xy}† (Nmm/mm)
BD30-1	0.254	5.397	2.833	4.756	3.474	-1.110
BD30-2	0.247	4.976	2.612	4.385	3.203	-1.023
BD30-3	0.270	4.334	2.275	3.819	2.790	-0.891
BD30-4	0.263	4.687	2.461	4.130	3.017	-0.964
BD30-5	0.296	4.507	2.366	3.972	2.901	-0.927
$\bar{x}$	0.266	4.780	2.510			
s_{n-1}	0.019	0.419	0.220			
CV (%)	7.06	8.76	8.76			

Table 6: Bending failure data for two-ply 30/-60 laminates († Values obtained from calculation).

$$f_{44}(M_x^2 + M_y^2) + f_{66}M_{xy}^2 = 1 \tag{26}$$

From which we obtain:

$$F_6 = \frac{1}{\sqrt{f_{66}}} = \frac{|M_{xy}|}{\sqrt{1 - f_{44}(M_x^2 + M_y^2)}} \tag{27}$$

However, there is a problem with this result because, as it will be seen in Section 4, the assumption of a quadratic interaction between M_x and M_y leads to poor results. Hence we will use the following modified equation to calculate F_6 (the reason for making this change will become clear in Section 5.2)

$$F_6 = \frac{1}{\sqrt{f_{66}}} = \frac{|M_{xy}|}{\sqrt{1 - f_{44}M_x^2}} \tag{28}$$

To evaluate F_6 we substitute into Equation 28 all data sets in Tables 5 and 6, and we find that the critical set of moment resultants that gives the smallest F_6 for flat ±45 and 30/-60 laminates is M_x = 2.790 Nmm/mm and M_{xy} = -0.891 Nmm/mm. The corresponding twisting strength is

$$F_6 = 1.10 \text{ Nmm/mm} \tag{29}$$

3.6. Combined Loading Strengths

This section presents the results obtained from tests involving multiple stress resultants.

3.6.1. In-Plane Strength

Table 7 lists the in-plane strengths measured for two-ply 30/-60 laminates.

Sample	$N_{x'}$ (N/mm)	N_x† (N/mm)	N_y† (N/mm)	N_{xy}† (N/mm)
TD30-1	45.69	34.27	11.42	19.78
TD30-2	45.44	34.08	11.36	19.68
TD30-3	45.53	34.15	11.38	19.72
TD30-4	48.01	36.01	12.00	20.79
TD30-5	50.62	37.97	12.66	21.92
$\bar{x}$	47.06	35.29	11.76	20.38
s_{n-1}	2.26			
CV (%)	4.80			

Table 7: Tensile failure data for two-ply 30/-60 laminate († Values obtained from calculation).

3.6.2. Coupled In-Plane and Bending Strength

Table 8 presents the failure strengths N_x measured from longitudinally curved specimens. The value of M_x was obtained from a four-point bending test, as explained in Section 2.6.2. In all of the tests from which these data were obtained failure occurred near the center of the sample.

Table 9 lists the values of N_x at failure for different set values of M_y, obtained from tension tests carried out on transversely curved samples. The transverse moment M_y was not measured during these tests but instead it was taken as the average for the curved specimens with the same initial curvature, in Table 8.

Sample	κ_x (1/mm)	N_x (N/mm)	M_x (Nmm/mm)
TBD90-D1.5-1	52×10^{-3}	68.96	1.986
TBD90-D1.5-2	52×10^{-3}	72.37	1.986
TBD90-D1.5-3	52×10^{-3}	81.52	1.986
TBD90-D1.5-4	52×10^{-3}	110.10	1.854
TBD90-D1.5-5	52×10^{-3}	93.75	1.722
TBD90-D2-1	40×10^{-3}	73.80	1.357
TBD90-D2-2	40×10^{-3}	81.17	1.265
TBD90-D2-3	40×10^{-3}	119.00	1.447
TBD90-D2-4	40×10^{-3}	86.12	1.327
TBD90-D2-5	40×10^{-3}	87.56	1.560
TBD90-D2-6	40×10^{-3}	99.25	1.600
TBD90-D2-7	40×10^{-3}	104.70	1.610
TBD90-D3-1	26×10^{-3}	108.20	0.989
TBD90-D3-2	26×10^{-3}	104.70	0.775
TBD90-D3-3	26×10^{-3}	103.90	0.743

Table 8: Tensile failure data for longitudinally curved two-ply 0/90 laminates. Note that $N_y = N_{xy} = M_y = M_{xy} = 0$.

Sample	κ_y (1/mm)	N_x (N/mm)	M_x † (Nmm/mm)	M_y (Nmm/mm)
TBD90-D2Y-1	40×10^{-3}	145.20	0.048	1.349
TBD90-D3Y-1	26×10^{-3}	136.80	0.031	0.836
TBD90-D3Y-2	26×10^{-3}	136.10	0.031	0.836

Table 9: Tensile failure data for transversely curved two-ply 0/90 laminates († Values obtained from calculation). Note that $N_y = N_{xy} = M_{xy} = 0$.

3.6.3. Coupled Shear and Twist Strength

Table 10 lists the force resultants in the loading direction at failure, together with the moment resultants required to straighten four curved samples with a longitudinal radius of curvature $r_{x'} =$ 38.1 mm.

Sample	$\kappa_{x'}$ (1/mm)	$N_{x'}$ (N/mm)	$M_{x'}$ (Nmm/mm)	$N_x = N_y = N_{xy}$† (N/mm)	$M_x = M_y = M_{xy}$† (Nmm/mm)
STD45-1	26×10^{-3}	42.42	0.043	21.21	0.022
STD45-2	26×10^{-3}	39.30	0.039	19.65	0.020
STD45-3	26×10^{-3}	42.04	0.042	21.01	0.021
STD45-4	26×10^{-3}	38.36	0.040	19.18	0.020
$\bar{x}$		40.53	0.041		
s_{n-1}		2.01	0.002		
CV (%)		4.95	4.45		

Table 10: Tensile failure data for longitudinally curved two-ply ±45 laminates († Values obtained from calculation). Note that $N_{y'} = N_{x'y'} = M_{y'} = M_{x'y'} = 0$.

3.6.4. Coupled Biaxial Bending Strength

Table 11 lists the failure curvatures that were measured by Yee. The corresponding moments have been calculated by substituting $\Delta\kappa_{x'} = \kappa_{x'}$, $\Delta\kappa_{y'} = \kappa_{y'}$, $\Delta\kappa_{x'y'} = 0$ into Equation 10. In the present case $\phi = 0$ and hence $x' = x, y' = y$.

$\kappa_x(1/mm)$	κ_y (1/mm)	M_x (Nmm/mm)	M_y (Nmm/mm)
0.20	0.100	5.046	2.658
0.20	0.067	5.016	1.840
0.21	0.050	5.249	1.428
0.21	0.040	5.240	1.180
0.20	0.033	4.986	0.998

Table 11: Bending failure curvatures from Yee[24] and calculated values of corresponding failure moments. Note that $M_{xy} = 0$.

3.6.5. Coupled Bending and Twist Strength

Table 12 lists seven combinations of moment resultants at failure, obtained by testing transversely curved two-ply ±45 samples. The moment resultants in the tow directions were calculated by following the same procedure described in Section 3.5, however note that in the present case $\Delta\kappa_{y'} = \kappa_{y'} \neq 0$.

4. Inadequacy of Quadratic Polynomial Criterion

The failure strengths obtained in Sections 3.1-3.5 are summarized in Table 13 and from these strengths the six coefficients that define the quadratic polynomial criterion can be calculated using Equations 8, thus fully defining the six-dimensional hyper-ellipsoid in Equation 2.

Sample	$\kappa_{x'}$ (1/mm)	$\kappa_{y'}$ (1/mm)	$M_{x'}$ (Nmm/mm)	$M_{y'}$ † (Nmm/mm)	$M_x = M_y$ † (Nmm/mm)	M_{xy} † (Nmm/mm)
BTD45-D2Y-1	0.314	40×10^{-3}	5.923	5.549	5.736	-0.187
BTD45-D2Y-2	0.339	40×10^{-3}	6.460	5.991	6.226	-0.234
BTD45-D3Y-1	0.304	26×10^{-3}	5.158	4.615	4.887	-0.271
BTD45-D3Y-2	0.330	26×10^{-3}	5.057	4.491	4.774	-0.283
BTD45-D3Y-3	0.302	26×10^{-3}	4.739	4.244	4.491	-0.248
BTD45-D3Y-4	0.272	26×10^{-3}	4.712	4.265	4.488	-0.224
BTD45-D3Y-5	0.268	26×10^{-3}	4.678	4.239	4.459	-0.219

Table 12: Bending failure data for transversely curved two-ply ±45 laminates († Values obtained from calculation). Note that $N_{x'} = N_{y'} = N_{x'y'} = M_{x'y'} = 0$.

Strength	Value
$F_{1t} = F_{2t}$ (N/mm)	133.60
$F_{1c} = F_{2c}$ (N/mm)	57.36
F_3 (N/mm)	16.91
$F_4 = F_5$ (Nmm/mm)	4.54
F_6 (Nmm/mm)	1.10

Table 13: Measured failure strengths of 2-ply 0/90 T300-1k/Hexcel 913 laminates.

At this point, the additional test data from Section 3.6 can be used to study the accuracy of this hyper-ellipsoid in defining a region of six-dimensional space in which no failure occurs. A visual check can be made by considering lower-dimensional sections of the ellipsoid that correspond to failure under in-plane loading, biaxial bending or in-plane-bending only conditions. It was found that the failure criterion works well the additional in-plane loading conditions, but it does not for the remaining two.

For example, Figure 11 is a plot of the test results involving in-plane and bending interactive failure obtained in Section 3.6.2, together with the results in Sections 3.1, 3.2, and 3.4. There are two sets of points in this plot, the experimentally obtained data points denoted by stars, and the corresponding points obtained by swapping x and y (in view of the symmetry of the laminate with respect to the material directions) denoted by circles. This plot shows that many failure data points lie inside the quadratic polynomial criterion. Also, the distribution of failure data points suggests that, instead of using a smooth, quadratic relationship to describe the interaction between N_x and M_x, a less continuous, e.g. polygonal, criterion would work better.

5. Alternative Failure Criterion

It has been shown in the previous section that a failure criterion defined by a single quadratic polynomial in six-dimensional stress resultant space does not work well for two-ply plain-weave laminates. We will now construct an alternative failure envelope inspired by a series of experimentally-based observations. Our approach is to consider three projections of the failure criterion, and for each projection to make use of the existing experimental evidence to propose a meaningful, physically based analytical description of the failure envelope. The three projections that are

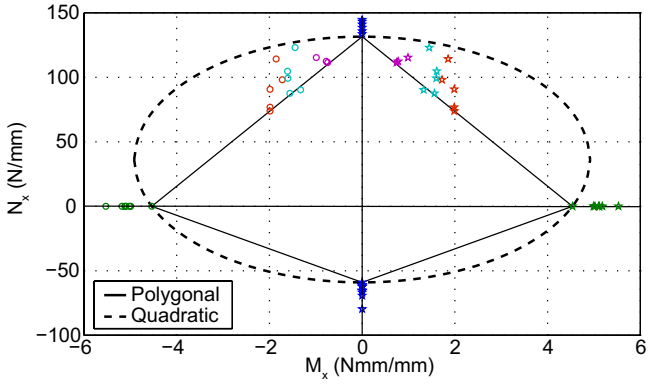

Figure 11: Axial-bending interaction.

considered correspond to: failure under pure in-plane loading, failure under biaxial bending and failure due to the interaction between in-plane and bending loads.

5.1. In-Plane Failure

In-plane failure has already been satisfactorily captured by the inequality

$$f_1(N_x + N_y) + f_{11}(N_x^2 + N_y^2) + f_{12}N_xN_y + f_{33}N_{xy}^2 < 1 \tag{30}$$

Figures 12a and 13a show the cross-sections of Equation 30 for $N_y = 0$ and N_{xy}= 0, respectively, along with the failure data points used to construct the locus. The off-axis tension test results presented in Section 3.6.1 have then been used to provide an independent check. This has been done in Figures 12b and 13b show the cross-sections of the locus when N_y = 11.77 N/mm and N_{xy} = 20.38 N/mm, respectively. Note that these figures present all of the failure points obtained from the off-axis tests, although the cross-sections were drawn for the average values of N_y and N_{xy}. In both figures all of the additional data points lie outside the locus which confirms that Equation 30 is a good choice.

5.2. Bending Failure

The results presented in Table 11 suggest that the value of M_x at failure is practically independent of the value of M_y. Hence, instead of considering the quadratic interaction that was assumed in the quadratic polynomial criterion in Equation 2, it is assumed that only the largest of the two bending moments is responsible for failure. Thus, for pure bending we define a square failure criterion bounded by $|M_x| = F_4$ and $|M_y| = F_5$. Figure 14 shows this square locus together with the experimental failure data in Table 11, denoted by stars, and the corresponding points obtained by swapping x and y and also reversing the signs of the moments, denoted by circles.

Next we consider the effects of a twisting moment M_{xy} in addition to the bending moments. has the effect of reducing the bending strengths in the tow directions. The experimental failure data from Tables 4, 5, 6 and 12, plotted in Figure 15, indicates that a good description of the reduction in twisting moment due to an applied bending moment is provided by a quadratic interaction.

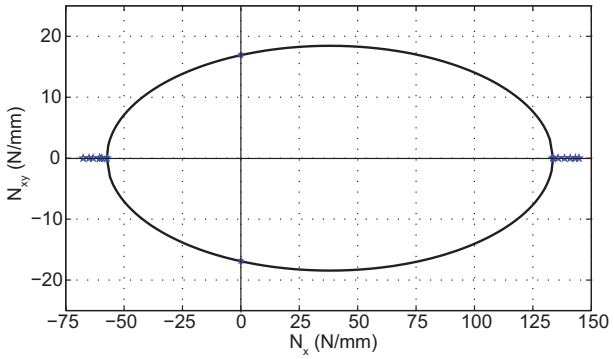

(a)

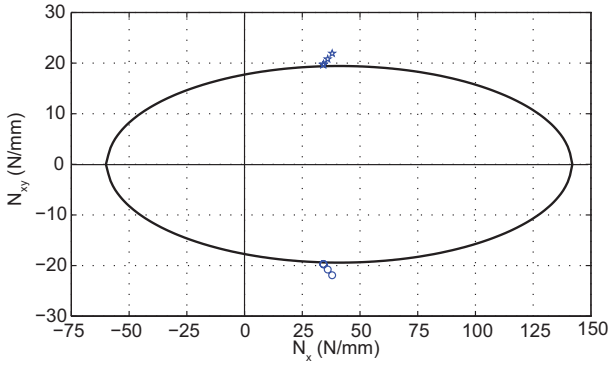

(b)

Figure 12: Axial-shear interaction for (a) $N_y = 0$ and (b) $N_y = 11.77$ N/mm.

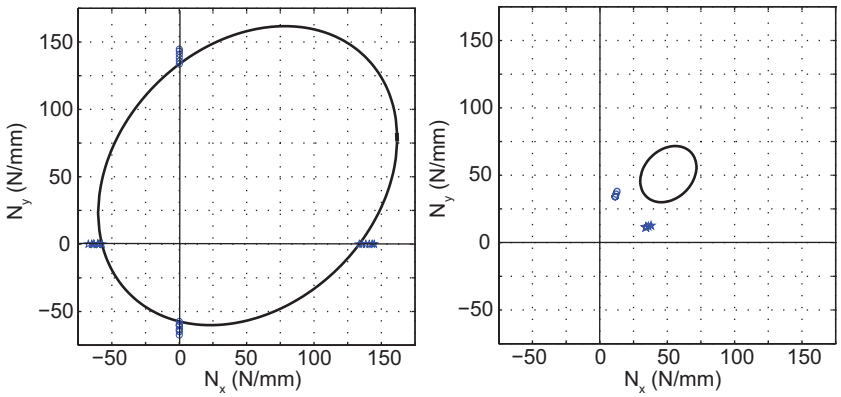

(a) (b)

Figure 13: Failure under biaxial in-plane loading for (a) $N_{xy} = 0$ and (b) $N_{xy} = 20.38$ N/mm.

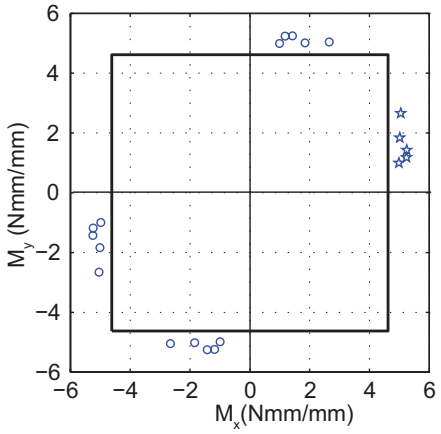

Figure 14: Biaxial bending failure locus.

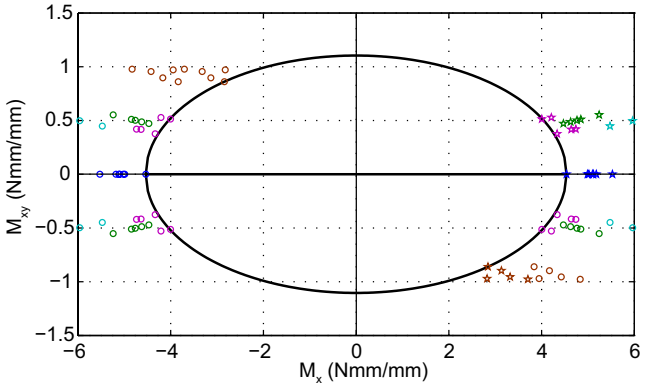

Figure 15: Bending-twisting interaction.

Hence, it is concluded that an accurate failure criterion for bending and twisting is defined by the following pair of inequalities:

$$\begin{cases} f_{44}M_x^2 + f_{66}M_{xy}^2 < 1 \\ f_{44}M_y^2 + f_{66}M_{xy}^2 < 1 \end{cases} \tag{31}$$

which can be written more compactly as

$$f_{44} \times \max(M_x^2, M_y^2) + f_{66}M_{xy}^2 < 1 \tag{32}$$

In three-dimensional moment resultants space, Equation 32 defines two cylinders with axes along M_x and M_y, hence the safe region defined by Equation 32 is the region defined by the intersection of these two cylinders.

5.3. In-Plane-Bending Failure

The tension tests performed on transversely curved specimens gave results, see Table 9, practically indistinguishable from the failure loads for pure tension, which suggests that the in-plane strength N_x does not change when a transverse moment M_y is applied. Similarly, the shear strength, see Table 10, remains practically unchanged when a twisting moment is applied. Thus it can be concluded that the only significant interaction to be captured is between in-plane and bending resultants of the same type, that is N_x interacts only with M_x and N_y interacts only with M_y. Figure 11 suggests that a linear interaction between $|N_x|$ and $|M_x|$ and, due to symmetry of the laminate, a linear interaction will also be assumed also between $|N_y|$ and $|M_y|$.

Hence, the third type of failure interaction is captured by the following inequalities:

$$\begin{cases} \dfrac{N_x}{F_x} + \dfrac{|M_x|}{F_4} < 1 \\ \dfrac{N_y}{F_y} + \dfrac{|M_y|}{F_4} < 1 \end{cases} \tag{33}$$

Here the in-plane failure strength F_x is calculated by imposing that Equation 33 matches Equation 30 when $M_x = M_y = 0$. Hence, we set $N_x = F_x$, replace $<$ with $=$ in Equation 30, and then solve the resulting quadratic equation for F_x. Similarly, F_y is obtained by setting $N_y = F_y$, etc. and then solving for F_y. Their expressions are as follows:

$$F_x = \frac{-(f_1 + f_{12}N_y) \pm \sqrt{(f_1 + f_{12}N_y)^2 - 4f_{11}(f_1N_y + f_{11}N_y^2 + f_{33}N_{xy}^2 - 1)}}{2f_{11}} \tag{34a}$$

$$F_y = \frac{-(f_1 + f_{12}N_x) \pm \sqrt{(f_1 + f_{12}N_x)^2 - 4f_{11}(f_1N_x + f_{11}N_x^2 + f_{33}N_{xy}^2 - 1)}}{2f_{11}} \tag{34b}$$

The pair of inequalities in Equation 33 can be written more compactly as

$$\max\left(\frac{N_x}{F_x}, \frac{N_y}{F_y}\right) + \frac{\max(|M_x|, |M_y|)}{F_4} < 1 \tag{35}$$

6. Summary and Discussion

We have proposed a failure criterion for two-ply plain weave laminates subjected to force and moment resultants. The criterion is defined by the set of three inequalities:

$$\begin{cases} f_1(N_x + N_y) + f_{11}(N_x^2 + N_y^2) + f_{12}N_xN_y + f_{33}N_{xy}^2 < 1 \\ f_{44} \times \max(M_x^2, M_y^2) + f_{66}M_{xy}^2 < 1 \\ \max\left(\dfrac{N_x}{F_x}, \dfrac{N_y}{F_y}\right) + \dfrac{\max(|M_x|, |M_y|)}{F_4} < 1 \end{cases} \tag{36}$$

and, defining the three failure indices (FI):

$$FI\#1 = f_1(N_x + N_y) + f_{11}(N_x^2 + N_y^2) + f_{12}N_xN_y + f_{33}N_{xy}^2 \tag{37a}$$

$$FI\#2 = f_{44} \times \max(M_x^2, M_y^2) + f_{66}M_{xy}^2 \tag{37b}$$

$$FI\#3 = \max\left(\frac{N_x}{F_x}, \frac{N_y}{F_y}\right) + \frac{\max(|M_x|, |M_y|)}{F_4} \tag{37c}$$

avoiding failure simply requires that all three failure indices be < 1.

This set of inequalities defines a six-dimensional region which is best visualized by considering a series of projections onto selected three-dimensional spaces, where each project explains about the interaction between a group of stress resultants. Thus, in Figure 16 we have considered in-plane failure, defined by FI#1=1, for which the failure criterion is an ellipsoid identical to the Tsai-Wu failure criterion, but expressed in terms of stress-resultants. Next, in Figure 17 we have considered failure due to bending and twisting moments, defined by FI#2=1, for which the failure criterion is formed by the intersection of two cylinders with axes along M_x and M_y. Note that when $M_{xy} = 0$ this locus reduces to the square seen in Figure 14.

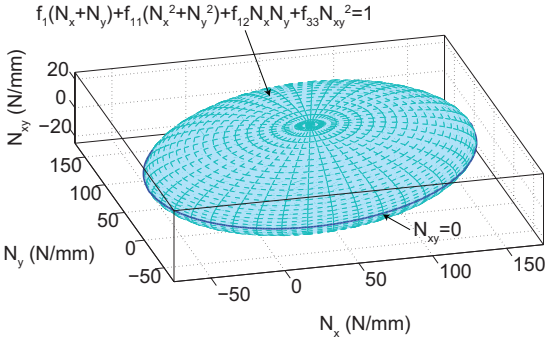

Figure 16: Failure criterion for in-plane forces.

The interactive nature of our failure criterion becomes apparent when we consider the envelope generated by FI#3=1, which defines the interaction between in-plane and bending effects. This interaction is illustrated by the seven projections in Figure 18. The interaction between N_x, N_y and M_x (and similarly, the interaction between N_x, N_y and M_y) in Figure 18a; it is described by two cones intersecting along an ellipse base. The interaction between M_x, M_y and N_x (and similarly, the interaction between M_x, M_y and N_y) is described by a rhombic prism whose

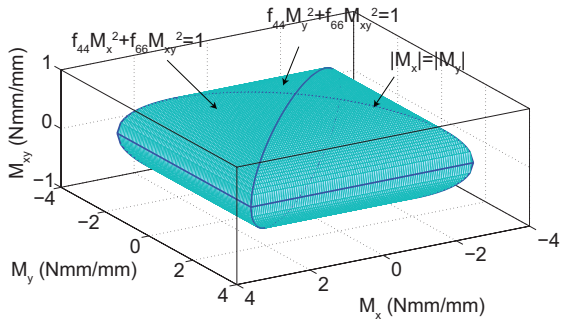

Figure 17: Failure criterion for bending and twisting moments.

faces are defined by the linear interaction between an axial force and the corresponding moment, Figure 18b; the distance between the two bases of this prism is related to the bending strength.

There is no interaction between shear and bending; hence the projection onto N_{xy}, M_x and M_y is a cuboid limited by the shear and bending failure strengths, Figure 18c. Similarly, there is no interaction between the axial strengths and the twisting strength, hence the N_x, N_y, M_{xy} projection is an elliptic cylinder, Figure 18d.

Lastly, the interaction between N_{xy}, M_x and M_{xy} is defined by an elliptic cylinder cut by the planes $N_{xy} = |F_3|$, Figure 18e. Similarly, the interaction between N_x, N_{xy} and M_{xy} is an elliptic cylinder cut by the planes $M_{xy} = |F_6|$, Figure 18f. Note that axis of this cylinder does not go through the origin due to the difference between tensile and compressive strengths. Lastly, the interaction between N_x, N_{xy} and M_x is defined by two cones intersecting along an ellipse, see Figure 18g.

Plastic failure criteria for thin cylindrical shells are well established [27, 28, 29] and our proposed failure criterion resembles Calladine's[27] locus for Tresca-type yielding, however in the present case the five strength properties of the laminate have to be measured from actual material tests. This approach required us to make the following two key assumptions. First that the micro-structure of the laminate does not change significantly (and hence its failure properties are unaffected) when manufacturing flat or curved laminates. This was a reasonable assumption since the weave wavelength is much shorter than the radius of curvature of the cylindrical shells that were tested. Second, the D matrix for the laminate, corrected by a single experimentally obtained coefficient, can be used to estimate the transverse moments at failure. Since, the initial curvature of any test sample can be measured before the test, the longitudinal curvature just before failure in the platen bending test can also be measured, and the corresponding transverse curvature is always approximately zero because any thin cylindrical shell tends to form cylindrical fold regions, in order to minimize mid-plane stretching. Hence, the transverse moment can be estimated using the D matrix of the laminate, however since this matrix has only been developed for the initial geometry of the laminate, a comparison was made of the measured longitudinal moment with the moment estimated using the same matrix and a 20% stiffness reduction was observed. The same reduction coefficient was then used in estimating the transverse moments. This stiffness reduction can be explained by the laminate thickness being reduced, due to the stretching of the tows making them flatter. Also, failure by delamination was not considered in this research, since this failure mode has not been observed in any laminate strength measurement

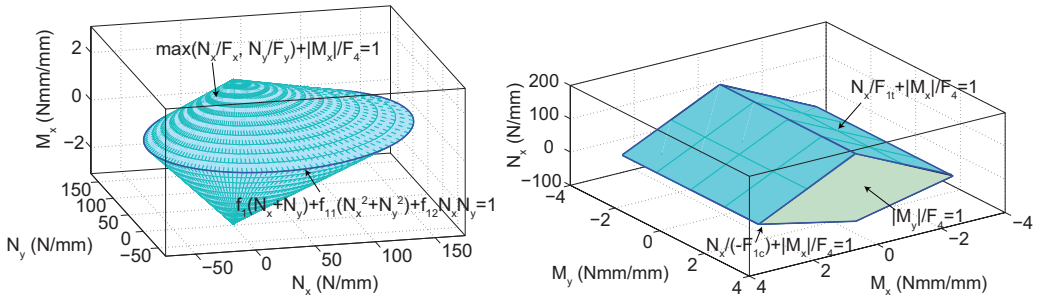

(a) N_x, N_y and M_x

(b) N_x, M_x and M_y

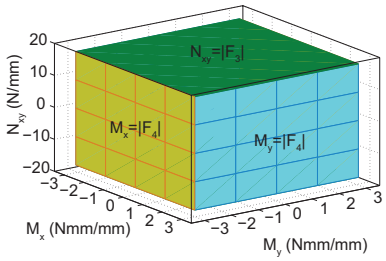

(c) N_{xy}, M_x and M_y

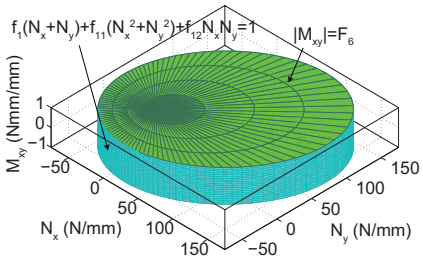

(d) N_x, N_y and M_{xy}

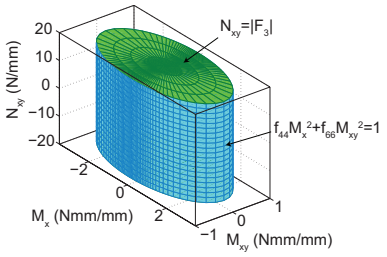

(e) N_{xy}, M_x and M_{xy}

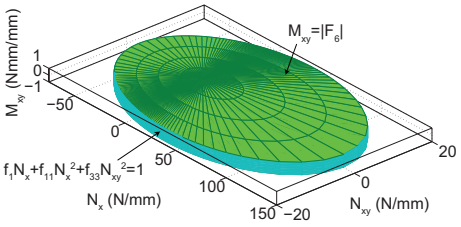

(f) N_x, N_{xy} and M_{xy}

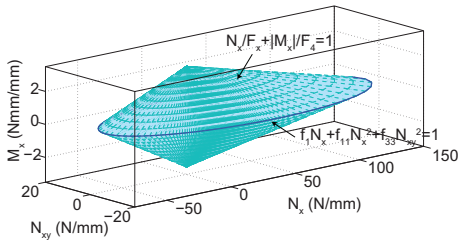

(g) N_x, N_{xy} and M_x

Figure 18: Interactions between in-plane and bending effects.

tests or indeed in any tests on tape-spring hinges [2, 30, 31].

The proposed failure criterion has a number of advantages over the quadratic polynomial considered in Karkkainen et al. [6] and Manne and Tsai [11], which results in a single hyper-ellipsoid. Most importantly it has successfully excluded unsafe regions of the stress resultant space, where the laminate is subjected to a combination of in-plane and bending stress resultants. Also, all material symmetries can be satisfied without having to reconcile any contradictions between directly obtained test data that provided five strength parameters.

7. Conclusion

This paper has presented a failure locus for a symmetric two-ply plain weave laminate in terms of force and moment resultants making a six dimensional loading space. Failure parameters were estimated from direct measurements through five sets of tests and five additional combined loading test configurations were tested to generate for validation.

Acknowledgments

We thank Dr Michael Sutcliffe (University of Cambridge, UK) for helpful discussions and Hexcel, UK for providing materials. HMYCM thanks the Cambridge Commonwealth Trust and the California Institute of Technology for financial support.

References

[1] M.J. Hinton, A.S. Kaddour, and P.D. Soden. *Failure criteria in fibre-reinforced-polymer composites, the world-wide failure exercise*. First edition, 2004.

[2] H.M.Y.C. Mallikarachchi and S. Pellegrino. Quasi-static folding and deployment of ultrathin composite tape-spring hinges. *Journal of Spacecraft and Rockets*, 48(1):187–198, 2011.

[3] H.M.Y.C. Mallikarachchi and S. Pellegrino. Deployment dynamics of composite booms with integral slotted hinges. *50th AIAA/ASME/ASCE/AHS/ASC Structures, Structural Dynamics, and Materials Conference*, Palm Springs, California, 4-7 May 2009.

[4] S.W. Tsai and E.M. Wu. A general theory of strength for anisotropic materials. *Journal of Composite Materials*, 5 (1):58–80, 1971.

[5] Z. Hashin and A. Rotem. A fatigue failure criterion for fibre reinforced materials. *Journal of Composite Materials*, 7:448–464, 1973.

[6] R.L. Karkkainen, B.V. Sankar and J.T. Tzeng. A direct micromechanical approach toward the development of quadratic stress gradient failure criteria for textile composites. *Journal of Composite Materials*, 41(16):1917–1937, 2007.

[7] T. Chou. *Microstructural design of fiber compoistes*. First edition, 1992.

[8] B.N. Cox, W.C. Carter, and N.A. Fleck. A binary model of textile composites: I - formulation. *Acta Metallurgica et Materialia*, 42(10):3463–3479, 1994.

[9] J. Whitcomb and K. Srirengan. Effect of various approximations on predicted progressive failure in plain weave composites. *Composite Structures*, 34(1):13–20, 1996.

[10] S. J. Song, A.M. Waas, K.W. Shahwan, O. Faruque and X.R. Xiao. Compression response of 2D braided textile composites: single cell and multiple cell micromechanics based strength predictions. *Journal of Composite Materials*, 42(23):2461–2482, 2008.

[11] P.M. Manne and S.W. Tsai. Design optimization of composites plates: Part i - design criteria for strength, stiffness, and manufacturing complexity of composite laminates. *Journal of Composite Materials*, 332(6):544–570, 1998.

[12] K.S. Liu and S.W. Tsai. A progressive quadratic failure criterion for a laminate. *Composite Science and Technology*, 58(7):1023–1032, 1998.

[13] J. E. Masters and M. A. Portanova. Standard test methods for textile composites. Contractor report 4751, National Aeronautics and Space Administration, Hampton, Virginia, 1996.

[14] ASTM Standard D6856-2003. *Standard guide for testing fabric-reinforced "textile" composite materials*. American Society for Testing and Materials, West Conshohocken, Pennsylvania, 2008.
[15] http://www.toraycfa.com/pdfs/T300DataSheet.pdf
[16] http://www.hexcel.com/Resources/DataSheets/Prepreg-Data-Sheets/913_eu.pdf
[17] ASTM Standard D3039/D3039M-2008. *Standard test method for tensile properties of polymer matrix composite materials*. American Society for Testing and Materials, West Conshohocken, Pennsylvania, 2008.
[18] N.A. Fleck and I. Sridhar. End compression of sandwich columns. *Composites: Part A*, 33(3):353–359, 2005.
[19] ASTM Standard D3518/D3518M-1994. *Standard test method for in-plane shear response of polymer matrix composite materials by tensile test of a ±45° laminate*. American Society for Testing and Materials, West Conshohocken, Pennsylvania, 2007.
[20] J.C.H. Yee and S. Pellegrino. Folding of woven composite structures. *Composites Part A-Applied Science and Manufacturing*, 36 (2): 273–278, 2005.
[21] T.W. Murphey, G.E. Sanford, and M.M. Grigoriev. Nonlinear elastic constitutive modeling of large strains in carbon fiber composite flexures. *16th International Conference on Composite Structures*, Porto, 2011.
[22] D.F. Adams, L.A. Carlsson, and R.B. Pipes. *Experimental characterization of advanced composite materials*. Third edition, 2003.
[23] J.C.H. Yee and S. Pellegrino, Biaxial bending failure locus for woven-thin-ply carbon fibre reinforced plastic structures. *46th AIAA/ASME/ASCE/AHS/ASC Structures, Structural Dynamics and Materials Conference*, Austin, TX, 2005, AIAA 2005-1811.
[24] J.C.H. Yee, Thin CFRP Composite Deployable Structures, PhD Dissertation, University of Cambridge, 2006.
[25] O. Soykasap. Micromechanical models for bending behaviour of woven composites. *Journal of Spacecraft and Rockets*, 43(5):1093–1100, 2006.
[26] G. Sanford, A. Biskner, and T.W. Murphey. Large strain behavior of thin unidirectional composite flexures. *51st AIAA/ASME/ASCE/AHS/ASC Structures, Structural Dynamics, and Materials Conference*, Orlando, Florida, 12-15 April 2010.
[27] C.R. Calladine. On the derivation of yield conditions for shells. *J. Appl. Mech.*, 39(3):852–853, 1972.
[28] P.G. Hodge Jr. The rigid-plastic analysis of symmetrically loaded cylindrical shells. *J. Appl. Mech.*, 21:336–442, 1954.
[29] A. Sawczuk and P.G. Hodge Jr. Comparison of yield conditions for circular cylindrical shells. *Journal of the Franklin Institute*, 269(5):362–374, 1960.
[30] H.M.Y.C. Mallikarachchi and S. Pellegrino. Optimized designs of composite booms with integral tape-spring hinges. *51st AIAA/ASME/ASCE/AHS/ASC Structures, Structural Dynamics, and Materials Conference*, Orlando, Florida, 12-15 April 2010.
[31] H.M.Y.C. Mallikarachchi and S. Pellegrino. Design and validation of thin-walled composite deployable booms with tape-spring hinges. *52nd AIAA/ASME/ASCE/AHS/ASC Structures, Structural Dynamics, and Materials Conference*, Denver, Colorado, 4-7 April 2011.